Review of the phenomenon of fluidization and its numerical modelling techniques

H. A. Khawaja*
Department of Engineering and Safety, UiT-The Arctic University of Norway, Tromsø, Norway

ABSTRACT

The paper introduces the phenomenon of fluidization as a process. Fluidization occurs when a fluid (liquid or gas) is pushed upwards through a bed of granular material. This may make the granular material to behave like a liquid and, for example, keep a level meniscus on a tilted container, or make a lighter object float on top and a heavier object sink to the bottom. The behavior of the granular material, when fluidized, depends on the superficial gas velocity, particle size, particle density, and fluid properties resulting in various regimes of fluidization. These regimes are discussed in detail in the paper. This paper also discusses the application of fluidized beds from its early usage in the Winkler coal gasifier to more recent applications for manufacturing of carbon nano-tubes. In addition, Geldart grouping based on the range of particle sizes is discussed. The minimum fluidization condition is defined and it is demonstrated that it may be registered slightly different when particles are being fluidized or de-fluidized. The paper presents discussion on three numerical modelling techniques: the two fluid model, unresolved fluid-particle model and resolved fluid particle model. The two fluid model is often referred to Eulerian-Eulerian method of solution and assumes particles as well as fluid as continuum. The unresolved and resolved fluid-particle models are based on Eulerian-Lagrangian method of solution. The key difference between them is the whether to use a drag correlation or solve the boundary layer around the particles. The paper ends with the discussion on the applicability of these models.

1. INTRODUCTION

Fluidization is a process in which granular material behaves like a liquid through suspension in a fluid, either gas or liquid. Fluidization occurs when a fluid (liquid or gas) is pushed upwards through a bed of granular material. As shown in Figure 1(a), at a low superficial gas velocity, the drag force on the particles is low (i.e. insufficient to balance the weight of the particles), and thus the bed remains in a packed state. At the critical value of the superficial gas velocity, known as the minimum fluidization velocity, the upward drag force balances the downward gravitational force on the particles; the particles become suspended in the fluid and the bed of material is said to be fluidized as shown in Figure 1(b). After fluidization, the pressure drop across the bed balances the net weight of the particles, i.e.,

*Corresponding Author: E-mail: hassan.a.khawaja@uit.no

$$\Delta P = \frac{M_s g}{A_c} \tag{1}$$

where ΔP is the pressure drop across the bed, M_s is the mass of solid particle in the bed, A_c is the cross-sectional area of the bed and g is the gravitational constant.

The behavior of a material, when fluidized, depends on the superficial gas velocity, particle size, particle density, and fluid properties. As shown in Figure 1(c), in some cases the fluidized bed expands uniformly once the fluid is passed through the granular particles. This state is

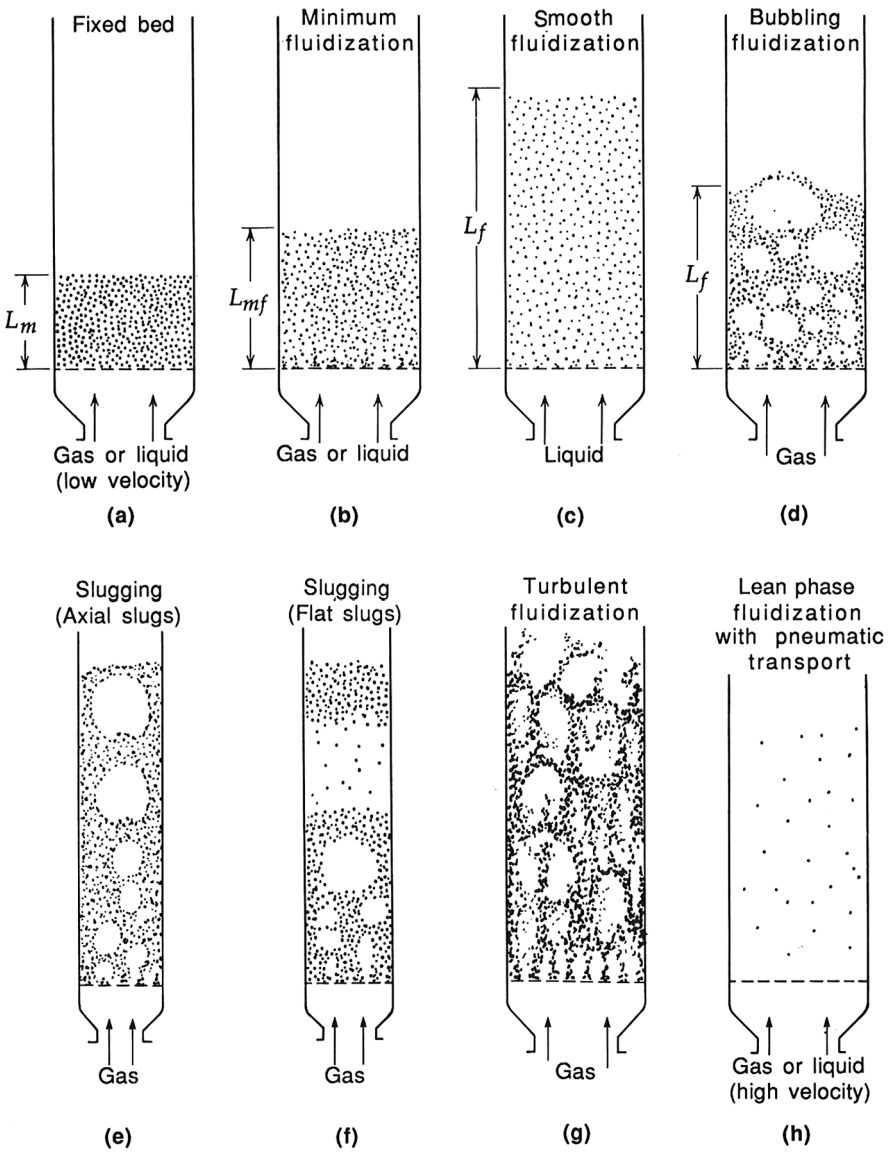

Figure 1: Regimes of fluidization: (a) fixed bed, (b) minimum fluidization, (c) smooth fluidization, (d) bubbling bed, (e) axial slugging bed, (f) flat slugging bed, (g) turbulent fluidization, (h) pneumatic transport [1]

known as uniform fluidization. Uniform fluidization usually occurs with very small particles fluidized by gas at relatively low superficial velocities, or with granular materials fluidized by a liquid. Granular material composed of larger particles (e.g. sand with a particle diameter > 250 μm) will bubble, without first passing through the uniform fluidization regime, when gas velocity exceeds the minimum fluidizing velocity as shown in Figure 1(d). The bubble sizes and frequency of formation of the bubbles depends on particle size, particle density, gas physical properties, and the size of the bed. With the increase of fluid velocity through the bed, the bubbling frequency increases hence there can be multiple bubbles in the bed at any given time. These bubbles start to coalesce to form bigger bubbles. When the size of the bubbles reaches the size of the cross-sectional area of the bed, a phenomenon called slugging is observed. Slugging may exhibit different forms with the shape of slugs depending on the particle and fluid properties, and on the cross-sectional shape of the bed. Figure 1(e) shows a form in which axial slugs have round edges. Alternatively, flat slugs can be formed, as shown in Figure 1(f). With increasing fluid velocity, the upper boundary of the bed becomes less distinct, and bubbles begin to break up. This phenomenon, known as turbulent fluidization, is shown in Figure 1(g). The transport of particles out of the bed, shown in Figure 1(h) is observed at very high gas velocities. In liquid fluidized beds, the transportation of particles occurs at slightly lower superficial velocities [1–3].

2. APPLICATION OF FLUIDIZED BEDS

Fluidized beds are currently used in many commercial processes. There are a number of advantages for particular applications. For example, fluidized beds provide uniform heat distribution avoiding hot spots and hence providing better control over reactions. This attribute is of great importance when a reaction has a narrow operating temperature. Fluidized beds also find applications in heat exchangers because of the high rate of heat transfer between particles, gas and immersed surfaces. Fluidized beds also have a large surface area between particle and gas (facilitating reaction between phases), and unlike a packed bed, may be relatively well mixed. Fluidized beds also offer better interaction between the solid and fluid phases. In fluidized beds, the particulate phase is able to move which adds into the mixing of phases and hence fluidized beds can sometimes be regarded as well mixed. This mixing coupled with the large thermal capacity of the particle phase enhances thermal transport inside the system and gives good heat transfer between the bed and its container. These aspects also help to maintain a homogeneous temperature field inside a fluidized bed. In addition, the pressure drop across the bed cannot exceed the weight of particles per unit bed area, which can reduce pumping costs.

The first large-scale commercial use of fluidized beds was seen in 1926 with the Winkler coal gasifier. In the Winkler process, coal was reacted with the steam and oxygen to produce synthesis gas for chemical industries. The general gasification reaction equation is shown in Equation (2).

$$3C\left(coal\right)_{(s)} + O_{2\,(g)} + H_2O_{(g)} \rightarrow 3CO_{(g)} + H_{2\,(g)} \tag{2}$$

The mixture of carbon monoxide and hydrogen generated is known as synthesis gas and can be used for energy production and other chemical reactions.

In this type of coal gasifier, a granular form of coal is screw fed into a fluidized bed chemical reactor. The coal is fluidized using a mixture of oxygen and steam. The ash and unreacted solids are collected at the bottom of the bed and product is collected from the top.

More commercial uses for fluidized beds were seen in the early 1940s. One common example is the Fluid Catalytic Cracking (FCC) process, which converts heavier petroleum

cuts into gasoline. In these systems, fluidized catalyst particles are shuttled between a fluidized bed reactor and a fluidized bed burner where coke deposits are burned off, generating heat for the endothermic cracking reaction. In the late 1970s, a fluidized bed process for the synthesis of polyethylene dramatically reduced the cost of this important polymer, making its use economical in many new applications. The polymerization reaction generates heat and the intense mixing associated with fluidization prevents hot spots in the reactor, where the polyethylene particles could melt. A similar process is used for the synthesis of polypropylene. With the high demand for gasoline, efforts were made in the 1950s to obtain liquid fuel out of natural gas (primarily methane) and from coal using fluidized bed technology. The fluidized bed are being used to obtain gasoline from coal in Fischer-Tropsch reactors especially in the coal rich countries. Fluidized beds are also being used for the production of Sulphur dioxide from Sulphur ore, the production of fertilizers (urea), the coating and growth of particles, and various synthesis reactions as well as biochemical reactions. Currently, most of the processes that are being developed for the industrial production of carbon nano-tubes use a fluidized bed. Fluidized beds are also used for drying because of their large capacity, good operability, low construction cost, and high thermal efficiency.

A new application of fluidization technology is chemical looping combustion, a process that can improve the effectiveness of carbon capture and storage. 'Carbon Capture and Storage' aims to mitigate the problems caused by emitting CO_2 from power stations combustion of carbonaceous fuels by removing the CO_2 and storing in geological formations. Regular combustion with air produces a flue gas that is mostly nitrogen (as air consists of about 78% nitrogen by volume), which hampers economic sequestration. Chemical looping uses a metal oxide as a solid oxygen carrier in a cyclic process. As shown in Equation (3), these metal oxide particles replace air (specifically oxygen in the air) as the oxidant in a combustion reaction,

$$(3n+1)\,MeO_{(s)} + C_nH_{2n+2\ (g)} \rightarrow (3n+1)\ Me_{(s)} + n\ CO_{2\ (g)} + (n+1)\,H_2O \tag{3}$$

$$2Me_{(s)} + O_{2\ (g)}\,(Air) \rightarrow\ 2MeO_{(s)} \tag{4}$$

Where *Me* is a metallic element such as iron (Fe).

The metal oxide particles react with a gaseous fuel in the fluidized bed, producing solid metal (or lower oxide) particles and a mixture of carbon dioxide and water vapor. The water vapor is condensed, leaving pure carbon dioxide that can be sequestered. As shown in Equation (4), the reduced solid metal particles must be re-oxidized so are circulated to another fluidized bed where they react with the air (specifically oxygen in the air), producing heat, before being reused in the combustor[1, 2, 4].

3. GELDART GROUPING

Geldart [5] proposed classifying particles into one of four groups, A, B, C and D. Geldart group A consists of particles with diameters between 20 and 100 μm; particle densities for group A particles are typically around 1400 kg/m^3. Fluidized beds with Geldart A particles will expand by a factor of 2 to 3 at incipient fluidization prior to the initiation of a bubbling bed phase. These particles are typically used in catalytic reactors. Geldart group B consists of the particles with diameters between 40 and 500 μm and particle densities between 1400

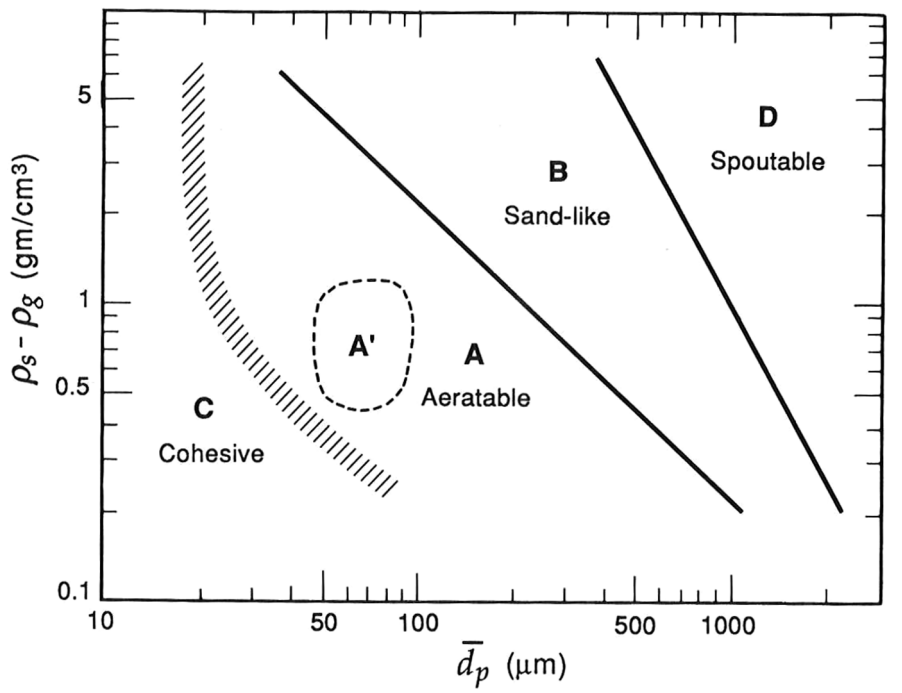

Figure 2: Geldart classification of particles; solid lines shows the boundaries of Geldart A, B and D groups; dotted line shows Geldart A particles for well-behaved FCC catalyst particles [6]; slotted lines shows the boundary between Geldart C and Geldart A group [1]

and 4500 kg/m^3. Bubbling in beds with Group B particles typically starts at incipient fluidization. Geldart group C contains extremely fine and subsequently the most cohesive particles. This group has a diameter range of 20 to 30 μm. These particles are difficult to fluidize and may require additional agitation. Geldart group D particles have diameters above 600 μm and typically have high particle densities. The fluidization of this group requires high fluid velocity and is usually associated with high levels of abrasion. Figure 2 shows the range of diameters and densities associated with the different Geldart groups.

4. MINIMUM FLUIDIZATION VELOCITY

The minimum fluidization velocity U_{mf} is the minimum superficial velocity of fluid needed to fluidize a bed [7]. The superficial velocity is the equivalent velocity of the fluid when there are no solid particles are present, as shown in Equation (5).

$$U_f = \epsilon V_f \tag{5}$$

Where U_f is superficial velocity, ϵ is the average voidage in the bed [8], and V_f is the average fluid velocity.

At minimum fluidization velocity, the net weight of the bed per unit area of the bed is balanced by the pressure drop across the bed as shown in Equation (6). Equation (6) shows that the pressure drop across the bed is equal to the weight of the solid particles per unit area in the fluidized bed less the buoyant force acted by the fluid on the solid particles.

$$\frac{\Delta P}{L_f} = \left(1-\epsilon_{mf}\right)\left(\rho_s - \rho_f\right) g \tag{6}$$

Where L_f is the length of fluidized bed, ρ_s is the density of solid particles, ρ_f is the density of the fluid, ϵ_{mf} is the voidage at minimum fluidization, and g is the gravity constant. The total mass of solids in the bed, M_s, (assuming that no solids are entrained and carried out of the bed) is shown in Equation (7).

$$M_s = \rho_s \left(1-\epsilon_{mf}\right) A_c L_f . \tag{7}$$

For the liquids and for the gases as long as the pressure drop is small, the fluid phase density remains constant. Hence, the right-hand side of Equation (6) is constant, and thus the pressure drop in a fluidized bed does not depend on the fluidizing velocity. In addition, experiments have shown that if a bed is densely packed then the pressure drop overshoots the fluidization pressure until the particles separate and fluidize as shown in Figure 3 (state A). Once the particles are fluidized, the fluidization curve follows same line for fluidization and de-fluidization as shown as state B in Figure 3 [9].

There are different relationships for pressure drop and minimum fluidization velocity based on which Geldart group of particles is being fluidized. [10] gives the following relationship for U_{mf} for Geldart A particles as shown in Equation (8).

$$U_{mf} = \frac{\epsilon_{mf}^3}{5\left(1-\epsilon_{mf}\right)^2} \frac{\Delta P}{S^2 \mu L_f} \tag{8}$$

Where S is the sphericity of the particles and μ is the kinematic viscosity of the fluid.

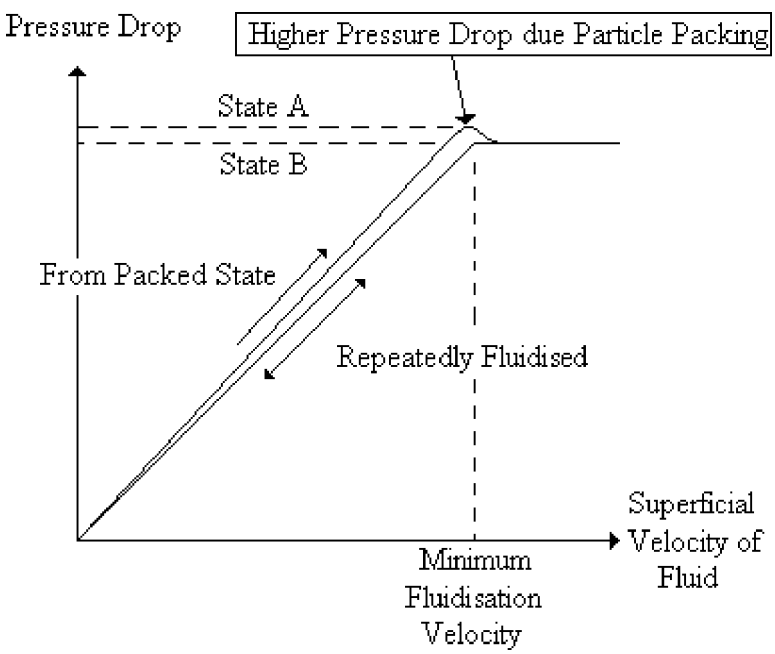

Figure 3: Pressure drop versus superficial velocity; the bed of solid particle has been fluidized from packed state, and repeatedly fluidized afterwards

For Geldart B and D particles, a commonly used relationship is given by [11] (based on the earlier attempts of [10, 12]) that can be used to calculate the U_{mf} as shown in Equation (9).

$$\frac{\Delta P}{L_f} = 150\left(\frac{\left(1-\epsilon_{mf}\right)^2}{\epsilon_{mf}^3}\right)\frac{\mu U_{mf}}{\left(Sd_p\right)^2} + 1.75\left(\frac{1-\epsilon_{mf}}{\epsilon_{mf}^3}\right)\left(\frac{\rho_f {U_{mf}}^2}{Sd_p}\right) \tag{9}$$

Where d_p is the diameter of the particles.

By introducing Reynolds number *Re* as:

$$Re = \frac{d_p U_{mf} \rho_f}{\mu} \tag{10}$$

and the Archimedes number *Ar* as:

$$Ar = \frac{d_p^3 \rho_f \left(\rho_s - \rho_f\right) g}{\mu^2} \tag{11}$$

and K_1 and K_2 as non-dimensional parameters as:

$$K_1 = \frac{1.75}{\epsilon_{mf}^3 S} \tag{12}$$

$$K_2 = \frac{150\left(1-\epsilon_{mf}\right)}{\epsilon_{mf}^3 S^2} \tag{13}$$

Equation (9) can be written as:

$$K_1 Re^2 + K_2 Re = Ar. \tag{14}$$

[13] gives the values of K_1 and K_2 over a range of particles for fluidization with Reynolds number between 0.001 and 4000, for Geldart A and B particles. Their values, shown in Table 1, predict minimum fluidization velocity with a maximum error of 34%. Similarly [14] also gives values of K_1 and K_2 for coarser particles such as Geldart B and D. A summary of values of K_1 and K_2 is given in Table 1.

Table 1: Values of non-dimensional parameters coefficients K_1 and K_2 for Equation (14)

Particle Size	$\frac{K_2}{2K_1}$	$\frac{1}{K_1}$
Fine [13] Geldart A and B	33.7	0.0408
Coarse [14] Geldart B and D	28.7	0.0494

5. NUMERICAL MODELLING TECHNIQUES

The science underlying the phenomena inside fluidized beds involves both fluid dynamics and the motion of particles. In order to simulate fluidized beds, both phenomena need to be modelled. In addition, it is essential to model the interaction between the two phases. In most cases, the fluid is modelled using the Eulerian method. The particles can be modelled using the Eulerian or the Lagrangian method. To simulate fluid behavior using the Eulerian method, the interaction with the particles is volume averaged, and the fluid motion is represented by a set of differential equations. The motion of the particles can be solved using the Lagrangian method by stepping the accelerations, velocities and displacements of each individual particle forward in time using Newton's second law of motion. The net force on each particle is computed by summing the forces due to contact with other particles [15], drag and buoyancy forces from the fluid as well as the force due to gravity. There are a number of techniques based on the combination of Eulerian and Lagrangian methods available to simulate solid-gas flow. [16] reviewed various gas-solid flow models as summarized in Table 2.

Each two-phase model shown in Table 2 shows a different combination of the method of solution for fluid and the solid particles. These models are Eulerian (resolved), Eulerian (unresolved) and Lagrangian.

The Eulerian (resolved) model solves for variables that are continuous over the domain. The domain is divided into a grid with the gradients and field values computed at the grid points. The Eulerian method is used for solving fluid dynamics problems e.g. a vector field for the velocity and scalar fields for density, pressure, etc. Two basic equations can describe the fluid flow. The continuity equation (conservation of mass) shown in Equation (15) and the Navier-Stokes equation (conservation of fluid momentum) as shown in Equation (16) [17, 18].

$$\frac{\partial \rho}{\partial t} + \nabla \cdot (\rho \vec{u}) = 0 \tag{15}$$

$$\frac{\partial \rho \vec{u}}{\partial t} + \nabla \cdot \left((u\ (\rho \vec{u}) \right) + \nabla p\ - \mu \nabla^2 \vec{u} - \rho g = 0 \tag{16}$$

Where ρ is the fluid density, $\vec{u}$ is the fluid velocity, p is the fluid pressure, μ is the fluid viscosity and g is the gravitational constant.

Table 2: Classification of various two-phase flow models [16]

	Model	Gas Phase	Solid Phase	Gas-Solid Coupling	Scale
1	Two-fluid Model	Eulerian	Eulerian	Gas-solid drag closures	Engineering (1m)
2	Unresolved Discrete Particle Model (Discrete Element Model)	Eulerian (unresolved)	Lagrangian	Gas-solid drag closures	Laboratory (0.01m)
3	Resolved Discrete Particle Model (Direct Numerical Simulation)	Eulerian (resolved)	Lagrangian	Boundary conditions at particle surface	Laboratory (0.01m)

For a fully resolved model, the fluid equations would be solved on a computational mesh around the particles, with the particles as solid boundaries. The drag, lift, etc. on the particles would arise from the pressure force and shear stress tensor integrated over the surface of the particle. This computational model of a two-phase system would require an Eulerian CFD simulation of the fluid flow around all of the particles, coupled with a Lagrangian method which tracks the motion of each particle [19]. This model is known as Resolved Discrete Particle Model and numbered three in Table 2. In practice, this model is very detailed and too computationally expensive to be used for practical systems [20]. Therefore, some compromises have to be made to simplify the physics in order to model the larger systems.

The 'Two-fluid model' is a Eulerian-Eulerian model. This model is particularly applicable to multi-fluid flows. This model can be extended to solid particles by volume averaging the motion of the solid particles such that they represent a continuum [21, 22]. These differential equations can be solved using Eulerian methods [23-25]. In this model, individual particle positions are not captured and thus certain features in the fluidized bed are unclear.

Both of the Eulerian-Lagrangian models mentioned are relatively expensive computationally as compared to the Eulerian-Eulerian model. However, the unresolved discrete particle model also known as Discrete Element Model (DEM) captures details of the particle motion, yet requires fewer computations than the fully resolved discrete particle model, so it can be used to model a laboratory scale fluidized bed. The advantage of using this model is that it provides greater detail on the behavior of the two-phase system with the additional capability to visualize each phase separately [26]. The unresolved Eulerian model solves for the volume averaged fluid velocity and density i.e. the mean value over a volume much larger than the size of the particles [27, 28]. Equations (15) and (16) can be volume averaged [21, 22]. The volume averaged continuity (mass conservation) equation is shown in Equation (17) and volume averaged Navier-Stokes (momentum conservation) equation is shown in Equation (18).

$$\frac{\partial(\rho\epsilon)}{\partial t} + \nabla \cdot (\rho\epsilon\ \vec{u}) = 0 \tag{17}$$

$$\frac{\partial(\rho\epsilon\ \vec{u})}{\partial t} + \nabla \cdot \left((u\ (\rho\epsilon\ \vec{u})\right) + \epsilon\nabla p - F_{drag} - \mu\nabla^2\epsilon\ \vec{u} - \rho\epsilon g = 0 \tag{18}$$

Where $\in$ is the voidage (the ratio of the fluid volume to the total volume) in the two-phase flow. Note that now closure expressions are needed to compute the drag force F_{drag}.

6. CONCLUSION

The science underlying the phenomena inside fluidized beds involves both fluid dynamics and the motion of particles. To simulate fluidized beds, both phenomena need to be modelled. In addition, it is essential to model the interaction between the two phases. The fluid is generally modelled using the Eulerian method. The particles can be modelled using the Eulerian or the Lagrangian methods summarized above (Table 2). The fundamental difference between the methods is the detail of the results and the scale of problem. Two-fluid model can model a commercial scale fluidized bed reactor, however, unresolved and resolved fluid-particle models are both currently too computationally expensive at this scale. Nonetheless, these models are more accurate and, therefore, are capable to shed light on the features of fluidization that are not yet fully understood. It is also to be noted that with the increase in computing performance, it will eventually be possible to use all of these models to solve for industrial scale fluidized bed problems.

REFERENCES

[1] Kunii, D. and Levenspiel, O., *Fluidization Engineering*. 1991: Butterworth-Heinemann.

[2] Lee, S., *Encyclopedia of Chemical Processing*. 2006: Taylor & Francis.

[3] Khawaja, H., *CFD-DEM and Experimental Study of Bubbling in a Fluidized Bed*. Journal of Computational Multiphase Flows, 2015. **In review**.

[4] Gupta, C. K. and Sathiyamoorthy, D., *Fluid Bed Technology in Materials Processing*. 1999: CRC Press.

[5] Geldart, D., *Types of gas fluidization*. Powder Technology, 1973. 7(5): pp. 285–292.

[6] Miyauchi, T., et al., *Transport Phenomena and Reaction in Fluidized Catalyst Beds*. 1981. pp. 275–448.

[7] Khawaja, H., *CFD-DEM Simulation of Minimum Fluidisation Velocity in Two Phase Medium*. The International Journal of Multiphysics, 2011. 5(2): pp. 89–100.

[8] Khawaja, H., et al., *Quantitative Analysis of Accuracy of Voidage Computations in CFD-DEM Simulations*. The Journal of Computational Multiphase Flows, 2012. 4(2): pp. 183–192.

[9] Davidson, J. F. and Harrison, D., *Fluidization Eds.,*. 1971: Academic Press, New York.

[10] Carman, P. C., *Fluid Flow Through Granular Beds*. Transactions - Institution of Chemical Engineeres, 1937. 15: pp. 150–166.

[11] Ergun, S., *Fluid flow through packed columns*. Chem. Process Eng. London, 1952. 1: pp. 89–94.

[12] Blake, F. C., *The resistance of packing to fluid flow*. Transactions of American Institute of Chemical Engineers, 1922. 14: pp. 415–421.

[13] Wen, C. Y. and Yu, Y. H., *Mechanics of fluidization*. Chem. Eng. Prog. Symp. Series., 1966(62): pp. 100–111.

[14] Chitester, D. C., et al., *Characterstics of Fluidization at High-Pressure*. Chemical Engineering Science, 1984. 39(2): pp. 253–261.

[15] Khawaja, H. and Parvez, K., *Validation of normal and frictional contact models of spherical bodies by FEM analysis*. The International Journal of Multiphysics, 2010. 4(2): pp. 175–185.

[16] van der Hoef, M. A., et al., *Numerical simulation of dense gas-solid fluidized beds: A multiscale modeling strategy*, in *Annual Review of Fluid Mechanics*. 2008, Annual Reviews: Palo Alto. pp. 47–70.

[17] Anderson, J. D., *Computational fluid dynamics: the basics with applications*. 1995: McGraw-Hill.

[18] Patankar, S. V., *Numerical Heat Transfer and Fluid Flow*. 1980: Taylor & Francis.

[19] Skodras, G., et al., *Simulation of a molten bath gasifier by using a CFD code*. Fuel, 2003. 82(15–17): pp. 2033–2044.

[20] Baryshev, G., Khawaja, H. and Moatamedi, M., *Optimization of Particle Search Algorithm for CFD-DEM Simulations*. The Journal of Computational Multiphase Flows, 2013. 5(3): pp. 223–230.

[21] Jackson, R., *The Dynamics of Fluidized Particles*. 2000: Cambridge University Press.

[22] Crowe, C. T., Sommerfeld, M. and Tsuji, Y., *Multiphase Flows With Droplets and Particles*. 1998: CRC Press.

[23] Lopes, R. J. G. and Quinta-Ferreira, R. M., *CFD modelling of multiphase flow distribution in trickle beds*. Chemical Engineering Journal, 2009. 147(2–3): pp. 342–355.

[24] Panneerselvam, R., Savithri, S. and Surender, G. D., *CFD simulation of hydrodynamics of gas–liquid–solid fluidised bed reactor.* Chemical Engineering Science, 2009. 64(6): pp. 1119–1135.

[25] Mazzei, L. and Lettieri, P., *CFD simulations of expanding/contracting homogeneous fluidized beds and their transition to bubbling*. Chemical Engineering Science, 2008. 63(24): pp. 5831–5847.

[26] Khawaja, H. and Scott, S., *CFD-DEM Simulation of Propagation of Sound Waves in Fluid Particles Fluidised Medium*. The International Journal of Multiphysics, 2011. 5(1): pp. 47–60.

[27] Xu, B. H. and Yu, A. B., *Numerical simulation of the gas-solid flow in a fluidized bed by combining discrete particle method with computational fluid dynamics*. Chemical Engineering Science, 1997. 52(16): pp. 2785–2809.

[28] Christensen, D., et al., *Insights in distributed secondary gas injection in a bubbling fluidized bed via discrete particle simulations*. Powder Technology, 2008. 183(3): pp. 454–466.